Lanthanide nano-drums: a new class of molecular nanoparticles for potential biomedical applications†

Richard A. Jones,[*a] Annie J. Gnanam,[a] Jonathan F. Arambula,[a]
Jessica N. Jones,[bc] Jagannath Swaminathan,[cd] Xiaoping Yang,[ae]
Desmond Schipper,[a] Justin W. Hall,[a] Lauren J. DePue,[a] Yakhya Dieye,[f]
Jamuna Vadivelu,[f] Don J. Chandler,[g] Edward M. Marcotte,[bcd]
Jonathan L. Sessler,[a] Lauren I. R. Ehrlich[bc] and Katherine A. Brown[ah]

We are developing a new class of lanthanide-based self-assembling molecular nanoparticles as potential reporter molecules for imaging, and as multi-functional nanoprobes or nanosensors in diagnostic systems. These lanthanide "nano-drums" are homogeneous 4d−4f clusters approximately 25 to 30 Å in diameter that can emit from the visible to near-infrared (NIR) wavelengths. Here, we present syntheses, crystal structures, photophysical properties, and comparative cytotoxicity data for six nano-drums containing either Eu, Tb, Lu, Er, Yb or Ho. Imaging capabilities of these nano-drums are demonstrated using epifluorescence, total internal reflection fluorescence (TIRF), and two-photon microscopy. We discuss how these molecular nanoparticles can to be adapted for a range of assays, particularly by taking advantage of functionalization strategies with chemical moieties to enable conjugation to protein or nucleic acids.

1. Introduction

"Nanodiagnostics" involves the use of engineered nanomaterials that can be biofunctionalized with target-specific molecules of interest, allowing ultra-

[a]*Department of Chemistry, The University of Texas at Austin, 105 E. 24th St. Stop A5300, Austin, Texas 78712, USA. E-mail: rajones@cm.utexas.edu; Tel: +1 512 471 1706*

[b]*Department of Molecular Biosciences, The University of Texas at Austin, Austin, Texas 78712, USA*

[c]*Institute for Cellular and Molecular Biology, The University of Texas at Austin, Austin, Texas 78712, USA*

[d]*Center for Systems and Synthetic Biology, The University of Texas at Austin, Austin, Texas 78712, USA*

[e]*College of Chemistry and Materials Engineering, Wenzhou University, Wenzhou 325035, China*

[f]*Department of Medical Microbiology, University of Malaya, Kuala Lumpur 50603, Malaysia*

[g]*Luminex, Austin, Texas, 78727, USA*

[h]*Cavendish Laboratory, Department of Physics, University of Cambridge, Cambridge CB3 0HE, UK*

† Electronic supplementary information (ESI) available. CCDC 921361–921363 and 1004328. For ESI and crystallographic data in CIF or other electronic format see DOI: 10.1039/c4fd00117f

sensitive detection. These materials include metal nanoparticles, DNA-based structures and circuits, nanowires and carbon nanotubes, quantum dots, and nanoporous materials.[1–3] Nanodiagnostic approaches are particularly prevalent in biomarker detection and imaging, and hold promise for facilitating the development of rapid, cost-effective, point-of-care diagnostics, which would be particularly attractive for implementations in both developing and developed countries.[3,4]

Many of these imaging and diagnostics applications rely upon the use of fluorescent dyes or labels as reporter molecules, because of their exceptional measurement contrast properties. However, both fluorescent dyes and protein-based fluorescent probes have technical limitations, including susceptibility to severe photo-bleaching (which limits long-term analysis), and small Stokes shifts. In comparison, lanthanide-based bioprobes have several advantages over conventional organic dyes or semiconductor quantum dots. These advantages include a very large pseudo-Stokes shift between the excitation and emission wavelengths, absence of photo-bleaching, long lived excited states, and narrow emission bands which enable selective detection.[5] The long emission lifetimes of lanthanide(III) complexes (1 μs to 5 ms) make them attractive bioprobes, because these lifetimes offer the possibility of using time-gated acquisition methods to enhance signal/noise by minimizing interference from light scattering or autofluorescence.[6–8]

As part of our research focused on high nuclearity lanthanide moieties, we recently reported a new class of luminescent high nuclearity self-assembled cadmium-lanthanide cluster molecules ("molecular nanoparticles") with unusual drum-like architectures.[9,10] In the current study, we have evaluated the potential of these molecules to serve as probes in biological applications. Our original report described nano-drum NIR emitters that featured Nd, Yb, Er, as well as Gd.[10] Since many lanthanide-based probes systems use Eu or Tb, which emit in the visible spectrum, we have also investigated the synthesis and photophysical properties of nano-drums based on these two metals. We describe here the synthesis of four new examples of molecular nano-drums, $[Ln_6Cd_{18}L_9Cl_8(OAc)_{28}]$ (Ln = Eu (**1**) and Tb (**2**)), $[Lu_6Cd_{18}L_9Cl_{10}(OAc)_{26}]$ (**3**), and $[Ho_8Cd_{24}L_{12}(OAc)_{48}]$ (**4**). We have structurally characterized each of these compounds by single crystal X-ray diffraction studies. We explore the potential of this class of compounds for biological applications by assessing their cytotoxicity using two cancer cell lines. We also investigate the imaging properties of nano-drums containing Er and Yb, which are analogues of **4**, using three microscopy platforms commonly used for visualization of cells and tissues: epifluorescence, TIRF, and two-photon microscopy.

2. Experimental

2.1 Synthesis of $[Ln_6Cd_{18}L_9Cl_8(OAc)_{28}]$ (Ln = Eu (1) and Tb (2)) and $[Lu_6Cd_{18}L_9Cl_{10}(OAc)_{26}]$ (3) and $[Ho_8Cd_{24}L_{12}(OAc)_{48}]$ (4)

All reactions were performed under dry oxygen-free dinitrogen atmospheres using standard Schlenk techniques. Metal salts and other solvents were purchased from Aldrich and used directly without further purification. The Schiff-base ligand H₂L (N,N'-bis(3-methoxysalicylidene)hexane-1,6-diamine) was prepared according to well-established procedures.[11] Melting points were obtained in sealed glass

capillaries under dinitrogen and are uncorrected. Complexes $[Er_8Cd_{24}L_{12}(OAc)_{48}]$ (**5**) or $[Yb_8Cd_{24}L_{12}(OAc)_{48}]$ (**6**) were prepared as previously described.[10]

$[Eu_6Cd_{18}L_9Cl_8(OAc)_{28}]$ (**1**). 0.52 mmol (0.1382 g) of $Cd(OAc)_2 \cdot 2H_2O$ and 0.12 mmol (0.0439 g) of $EuCl_3 \cdot 6H_2O$ were dissolved in 60 mL MeOH at room temperature, and 0.26 mmol (0.1001 g) H_2L and 0.30 mmol Et_3N in 10 mL EtOH were then added. The resulting solution was stirred and heated under reflux for 30 min, allowed to cool, and then filtered. Diethyl ether was allowed to diffuse slowly into the filtrate at room temperature and pale yellow crystals were obtained after one week. The crystals were filtered off and washed with EtOH (5 mL). Yield (based on $EuCl_3 \cdot 6H_2O$): 0.0926 g (52%). m. p. > 175 °C (dec.). ^{1}H NMR (600 MHz, CD_3OD): δ (ppm) −19.644 (2H), −19.349 (2H), −13.287 (2H), −9.285 (4H), −2.337 (4H), −2.245 (12H), −1.767 (4H), −1.546 (2H), −1.417 (18H), −0.805 (6H), −0.636 (4H), 0.337 (2H), 0.479 (12H), 0.660 (6H), 0.863 (4H), 0.991 (8H), 1.075 (20H), 1.140 (10H), 1.201 (12H), 1.261 (6H), 1.449 (12H), 1.903 (12H), 2.023 (2H), 2.118 (2H), 3.592 (6H), 3.657 (6H), 3.856 (6H), 4.231 (12H), 4.495 (4H), 4.634 (4H), 4.890 (12H), 5.168 (6H), 5.438 (4H), 5.524 (8H), 6.184 (4H), 6.426 (4H), 6.780 (2H), 6.879 (4H), 6.912 (2H), 8.321 (2H), 9.642 (4H), 10.372 (4H), 11.252 (12H), 12.511 (12H), 12.929 (4H), 13.117 (8H), 13.344 (4H), 14.607 (12H), 16.249 (4H). IR (CH_3OH, cm^{-1}): 2930 (w), 1632 (m), 1572 (s), 1465 (m), 1408 (s), 1307 (m), 1212 (s), 1079 (w), 1017 (w), 850 (m), 734 (s).

$[Tb_6Cd_{18}L_9Cl_8(OAc)_{28}]$ (**2**). The procedure was the same as that for **1** using $TbCl_3 \cdot 6H_2O$ (0.0448 g, 0.12 mmol). Pale yellow single crystals of **2** were formed after one week. Yield: 0.062 g (35%). m. p. > 184 °C (dec.). ^{1}H NMR (600 MHz, CD_3OD. The numbers of protons cannot be determined.): δ (ppm) −57.144, −52.939, −44.543, −26.494, 1.164, 1.485, 1.932, 2.136, 3.317, 3.444, 3.620, 3.892, 4.085, 6.629, 6.808, 6.913, 7.212, 8.354, 9.939, 12.594, 13.139, 21.931, 23.010, 25.508, 26.425, 35.846, 37.827, 50.759, 64.747, 78.970, 81.387, 94.693, 133.359. IR (CH_3OH, cm^{-1}): 2933 (m), 2851 (m), 1631 (s), 1602 (w), 1548 (w), 1456 (s), 1412 (m), 1303 (m), 1237 (m), 1213 (s), 1074 (m), 1025 (w), 849 (m), 741 (s).

$[Lu_6Cd_{18}L_9Cl_{10}(OAc)_{26}]$ (**3**). The procedure was the same as that for **1** using $LuCl_3 \cdot 6H_2O$ (0.0467 g, 0.12 mmol). Pale yellow single crystals of **3** were formed after one week. Yield: 0.053 g (30%). m. p. > 174 °C (dec.). ^{1}H NMR (600 MHz, CD_3OD. The numbers of protons cannot be determined.): δ (ppm) 0.762, 1.010, 1.119, 1.153, 1.116, 1.247, 1.452, 1.860, 1.889, 1.908, 1.945, 1.975, 2.070, 2.116, 2.153, 2.272, 2.304, 2.365, 2.401, 2.848, 2.892, 2.923, 2.986, 3.152, 3.430, 3.439, 3.600, 3.660, 3.713, 3.791, 3.854, 3.891, 3.948, 6.454, 6.515, 6.685, 6.777, 6.876, 6.906, 6.977, 7.132, 7.198, 7.322, 7.440, 7.615, 7.675, 7.936, 8.184, 8.326, 9.919, 10.983, 13.850 (br). IR (CH_3OH, cm^{-1}): 2934 (w), 1635 (s), 1579 (s), 1549 (s), 1452 (s), 1406 (s), 1307 (m), 1238 (m), 1213 (s), 1080 (m), 742 (s).

$[Ho_8Cd_{24}L_{12}(OAc)_{48}]$ (**4**). $Ho(OAc)_3 \cdot 4H_2O$, (0.0497 g, 0.12 mmol), $Cd(OAc)_2 \cdot 2H_2O$, (0.1384 g, 0.52 mmol) and H_2L (0.1000 g, 0.26 mmol) were dissolved in MeOH (25 mL) at room temperature and Et_3N (1 mL) added. The resulting solution was stirred and heated under reflux for 30 minutes. After cooling to room temperature, the solution was filtered and the filtrate transferred to test tubes. Diethyl ether vapour was allowed to diffuse slowly into the filtrate at room temperature and pale yellow crystals were obtained after one week. The crystals were filtered off and washed with MeOH (2 mL). Yield (based on $Ho(OAc)_3 \cdot 4H_2O$): 0.0823 g (48%). m. p. > 178 °C (dec.). IR (CH_3OH, cm^{-1}): 2932

(w), 1889 (w), 1634 (m), 1574 (s), 1435 (s), 1307 (m), 1169 (w), 1213 (s), 1080 (m), 1044 (w), 962 (s), 873 (s), 818 (w), 742 (s), 669 (m), 641 (w).

2.2 X-ray structure determinations

Powder X-ray diffraction data were collected on a Rigaku R-AXIS RAPID II. Single crystal data were collected on a Rigaku Saturn Kappa CCD diffractometer with graphite monochromated Mo-Kα radiation ($\lambda = 0.71073$ Å) at 223 K. The data set was corrected for absorption based on multiple scans and reduced using standard methods. Data reduction was performed using DENZO-SMN.[12] The structures were solved by direct methods and refined anisotropically using full-matrix least-squares methods with the SHELX 97 program package.[13] Coordinates of the non-hydrogen atoms were refined anisotropically, while hydrogen atoms were included in the calculation isotropically but not refined. Neutral atom scattering factors were taken from Cromer and Waber.[14] Crystallographic data for all complexes are given in the ESI in Table S1† and selected bond lengths and angles are given in Tables S2–S4.†

2.3 Bead preparation

Polystyrene beads (6 μm, crosslinked) were suspended in a 50 : 50 (v/v) solution of methanol and chloroform in a 1.5 mL microfuge tubes. Typically 0.5–1 mg of compound was added and the suspension was then rotated from 2–4 days to permit bead loading. Suspensions were then dried under vacuum overnight and beads removed and then washed and re-suspended in phosphate buffered saline (PBS) prior to imaging.

2.4 Spectroscopic characterization

Physical measurements were made using the following instrumentation: NMR: VARIAN UNITY-plus. 600 spectrometer (^{1}H, 600 MHz) at 298 K in CD$_3$OD; IR: Nicolet IR 200 FTIR spectrometer. Absorption spectra were obtained on a BECKMAN DU 640 spectrophotometer, excitation and visible emission spectra on a QuantaMaster PTI fluorimeter. Fluorescence quantum yields were determined by using quinine sulfate ($\Phi_{em} = 0.546$ in 0.5 M H$_2$SO$_4$) and [Ru(bipy)$_3$]Cl$_2$ (bipy = 2,2'-bipyridine; $\Phi_{em} = 0.028$ in water) as standard for the Tb^{3+} and Eu^{3+} complexes, respectively.[15]

X-ray photoelectron spectra (XPS) were obtained using a Kratos AXIS Ultra spectrometer equipped with a monochromatized Al Kα source, hybrid optics, and a delay line detector coupled to a hemispherical analyzer. The analysis chamber base pressure was typically 2×10^{-9} Torr. All spectra were recorded using a single sweep with a spot size of 300 μm $\times$ 700 μm. Survey scans were collected from 0–1200 eV with a pass energy of 80 eV, step size of 1 eV, and a dwell time of 250 ms. The high resolution component spectra were collected with a pass energy of 20 eV, step size of 0.1 eV, and a dwell time of 3600 ms. Binding energies were referenced to the adventitious carbon line (C 1s, 284.8 eV) and a charge neutralization was applied during all acquisitions. Casa XPS analysis software was used for stoichiometry determination of the samples and Kratos sensitivity factors used for each element of interest. All samples were washed with methanol three times and dried under vacuum for 18 hours before placing in an Al cup within the XPS instrument.

Samples were carefully spread evenly within the cup using a blunt tool covered with Al foil between each procedure to avoid contamination.

2.5 Cytotoxicity assays

The proliferation of exponential phase cultures was carried out using either an A549 or an AGS cancer cell line. A549 cells were seeded in 96-well microliter plates at 1000 cells per well and allowed to adhere overnight in 100 μL RPMI 1640 medium supplemented with 2 mM L-glutamine, 10% heat inactivated fetal bovine serum, and antibiotics (200 U cm^{-3} penicillin and 200 μg cm^{-3} streptomycin). AGS cells were seeded in 96-well microliter plates at 8000 cells per well, grown in F-12 medium supplemented with 10% heat inactivated fetal bovine serum, 100 U mL^{-1} penicillin, and 100 μg mL^{-1} streptomycin, and allowed to adhere for 1 day. Cell viability was assessed by tetrazolium salt reduction. Stock solutions of [Ho$_8$Cd$_{24}$L$_{12}$(OAc)$_{48}$] (**4**), holmium acetate, or H$_2$L ligand (all 5 mM) in 50/50 methanol–water were formulated and then diluted in medium for secondary stocks of 20–200 μM depending on the complex being tested. Secondary stock solutions were serially diluted in medium and immediately added to wells, whereupon plates were incubated at 37 °C under a 5% CO$_2$/95% air atmosphere. After a total of 3 days, a 50 μL aliquot of 3 mg mL^{-1} tetrazolium dye, 3-(4,5-dimethylthiazol-2-yl)-2,5-diphenyltetrazolium bromide (MTT, Sigma Chemical), was added to each well, followed by a 4 hour incubation at 37 °C. The medium was then removed and the resulting formazan was dissolved in 50 μL DMSO and absorbances measured at 560–650 nm using a microplate reader (Molecular Devices, Sunnyvale, CA). Absorbances were corrected for background and the values normalized to wells containing untreated cells to allow plate-to-plate comparison. The data are shown as mean inhibition of proliferation or growth as a percentage of control cells' proliferation or growth from 2–3 replicate values.

2.6 Microscopy

A flow chamber was constructed from a pre-cleaned glass slide and coverslip joined by double-sided sticky tape. About 1 mg of Yb and Er loaded beads were suspended in 20 μL of water and loaded in the flow chamber, which was used for both the epifluorescent and TIRF imaging. For epifluorescent imaging, the slide was mounted on a Nikon Eclipse TE2000-E inverted microscope (Nikon Inc, Japan) and images of the beads acquired at 1 frame per second using a Cascade II 512 camera (Photometrics, Tucson, AZ) on a Nikon Apo 60×/NA 0.95 objective. A combination of excitation filters DAPI – AT350/50× (340–380 nm), FITC – ET490/20× (465–495 nm) or TRITC – ET555/25× (528–553 nm) and emission filters DAPI – ET460/50 m (435–485 nm), FITC – ET525/36 m (515–555 nm), TRITC – ET605/52 m (590–650 nm) or Cy5 – ET700/60× (640–730 nm) were used to determine the capability of imaging the lanthanide dyes. The Sutter Lambda 10-3 filter wheels (Sutter Instrument, Novato, CA), motorized stage (Prior Scientific Inc; Rockland, MA), and image analysis were driven by Nikon NIS Elements Imaging Software.

TIRF imaging was performed in the objective mode using a Nikon Apo 60×/NA 1.49 oil objective set on a Nikon Eclipse Ti inverted microscope, fitted with a ProScan II motorized stage (Prior Scientific Inc; Rockland, MA) and a monolithic laser launch unit (Agilent Technologies; Santa Clara, CA) that is capable of providing tunable power and wavelength. The beads were excited by a 405 nm

laser at 2 mW power (at source of fiber optic) and the images acquired using an EMCCD iXon 3 camera (Andor; Belfast, UK) at 1 frame per second exposures before being filtered by a TIRF Quad Cube (Chroma Technology, Bellows Falls, VT). The Quad band filter is a setup of BandPass filters and dichroics that allow for 405/488/561/647 +/−10 nm excitation and emission between 417–476 nm, 500–547 nm, 574–620 nm, and 637–670 nm.

Two-photon fluorescence microscopy images were acquired with an Ultima IV microscope using PrairieView acquisition software and an Olympus Plan FL 20× water immersion objective (Prairie Technologies; Middleton, WI). Cells and beads were illuminated with a MaiTai Ti:sapphire laser (SpectralPhysics; Santa Clara, CA) tuned to 760 nm, or scanned from 690–1000 nm in 10 nm steps. Emitted light was passed through 400/50 nm, 480/40 nm, 535/50 nm, and 607/45 nm bandpass filters (Chroma Technology; Bellows Falls, VT) to separate PMTs for detection.

3. Results

3.1 Synthesis and X-ray structures of nano-drums

Reactions of the flexible Schiff base ligand H_2L (Fig. 1) with $Cd(OAc)_2 \cdot 4H_2O$ and $LnCl_3 \cdot 6H_2O$ (Ln = Eu, Tb and Lu) in refluxing MeOH/EtOH produced yellow solutions from which the Cd–Ln complexes **1–3** were isolated as pale yellow crystalline solids in 52%, 35% and 30% yields, respectively. The larger 32-metal holmium complex **4** is isomorphous with the analogous Nd, Yb, and Er nano-drums reported recently[10] and was prepared in a similar fashion using $Ho(OAc)_2 \cdot 4H_2O$. Complexes **1** and **2** are isomorphous, and reveal a 24-metal drum-like structure. A key factor affecting the nano-drum self-assembly process is the use of the flexible Schiff-base ligand H_2L, which facilitates construction of the nano-drum. The central six carbon chains of the ligands form the sides of the drum, while the deprotonated phenolic oxygen atoms, imine nitrogen and methoxy oxygen atoms bind the metals at the top and bottom of the drum.

Two views of the crystal structure of **1** are shown in Fig. 2. The complex is of nanoscale proportions (16 × 21 × 21 Å). The ends of the drum are created by two rings of 12 metals (3 Eu(III) and 9 Cd(II)) coordinated to half of the N, O binding groups of the 9 Schiff base ligands, plus 14 OAc^- and 4 Cl^- units. The sides of the drum are formed by the $-(CH_2)_6-$ linkers of the Schiff base ligands. Each Schiff base ligand is thus coordinated to metals at both ends of the drum. In each 12-metal ring, three Eu ions are eight-coordinate. Two Eu(III) ions (Eu(1) and Eu(2)) have similar coordinate environments and each is bound by two Schiff base ligands and four bridging OAc^- anions. A bridging Cl^- anion replaces an acetate OAc^- in the coordinate environment of the third Eu(III) ion, (Eu(3)). For the nine Cd^{2+} ions, four of them (Cd(2), Cd(4), Cd(6) and Cd(9)) have bi-pyramidal
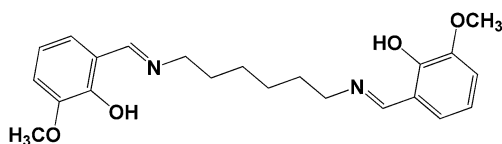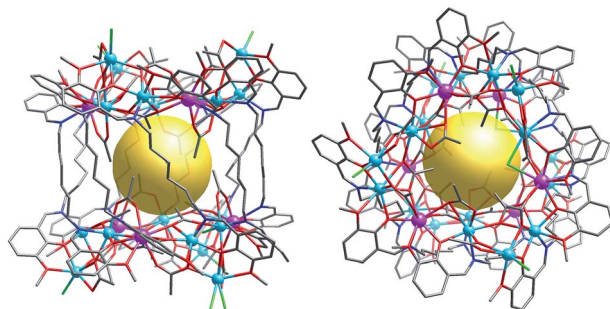

Fig. 1 Schiff base ligand H_2L.

Fig. 2 A view of the crystal structure of **1**. Viewed along the *a*-axis (left) and *c*-axis (right) (Eu^{3+}: purple; Cd^{3+}: blue).

geometries. They are coordinated to one Schiff base ligand, one Cl^- anion, and two (or three) OAc^- anions. The other five Cd^{2+} ions are seven-coordinate: three of them (Cd(1), Cd(3) and Cd(7)) are bound by two Schiff base ligands and two OAc^- anions, while two of them (Cd(5) and Cd(8)) are coordinated to one Schiff base and four OAc^- anions (ESI†).

The drum-like architecture of complex **3** is *mm* symmetric, formed by two equivalent 12-metal rings ($Lu_3Cd_9Cl_5(OAc)_{13}$) linked by nine Schiff base ligands (Fig. S1, ESI†). The slight difference between **1** and **2** *vs.* **3** is that, in **3**, one bridged Cl^- anion replaces a tridentate OAc^- anion. In **1–3**, each Ln^{3+} ion and its closest two Cd^{2+} ions are linked by phenolic oxygen atoms of L^{2-}, OAc^- anions and Cl^- anions. The average distances between Ln^{3+} and Cd^{2+} ions are 3.675 Å, 3.671 Å and 3.669 Å for **1**, **2** and **3**, respectively. Powder XRD patterns of **1–3** are similar to their simulated patterns generated from single crystal X-ray data (Fig. S2†).

Two views of the crystal structure of the 32-metal Ho–Cd drum $[Ho_8Cd_{24}L_{12}(OAc)_{48}]$ (**4**) are shown in Fig. 3. The ends of the drum are created by two rings of 16 metals (4 Ho(III) and 12 Cd(II)) coordinated to half of the N, O binding groups of the 12 Schiff base ligands plus 24 OAc^- anions. The sides of the drum are formed by the $-(CH_2)_6-$ linkers of the Schiff base ligands. Each Schiff base ligand is thus coordinated to metals at both ends of the drum. In each 16-metal ring, four Ho ions are eight-coordinate. For the 12 Cd^{2+} ions, four of them have bipyramidal geometries, and the other eight Cd^{2+} ions are seven-coordinate. Detailed descriptions of the structures of the isomorphous Er and Yb analogs of **4** are given in ref. 10.

3.2 Spectroscopic characterization

^{1}H NMR spectra of **1** and **2** in CD_2Cl_2 contain multiple broad peaks ranging from −20 to +18 ppm and −70 to +140 ppm, respectively, while **3** shows a narrower range of 0.7–14 ppm due to the diamagnetic Lu^{3+} ion. The ^{1}H NMR spectra of **1–3** remain unchanged for several weeks, indicating that they are stable in solution (Fig. S3–S5†). The photophysical properties of **1** and **2** were studied in CH_3CN. The free ligand H_2L exhibits absorption bands at 226, 260 and 327 nm which are all red-shifted upon coordination to metal ions in **1–3** (Fig. S6†). Complexes **1–3** exhibit similar solution absorption spectra. For the free ligand H_2L, excitation of the absorption band at 410 nm produces a broad emission band at $\lambda_{max} = 515$ nm
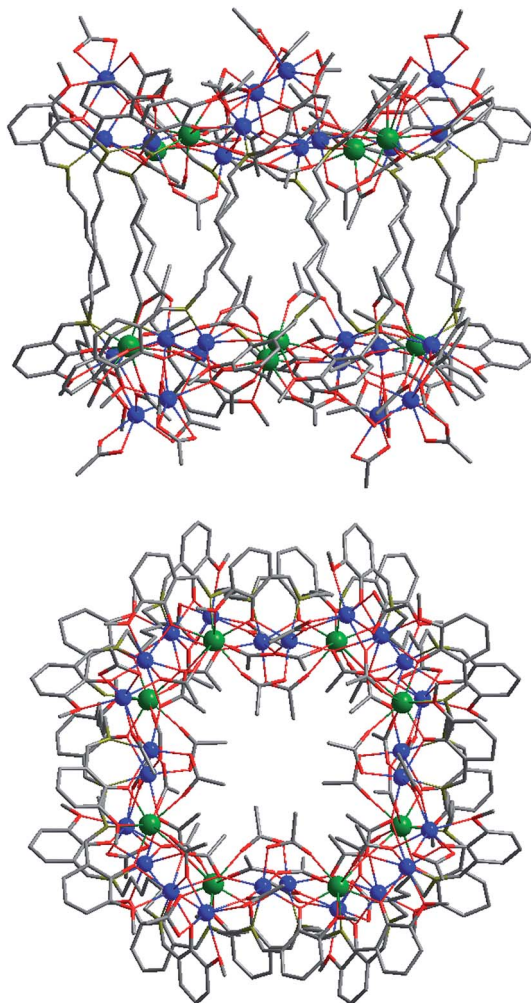
Fig. 3 A view of the crystal structure of 4. Viewed along the a-axis (top) and c-axis (lower). (Ho^{3+}: green; Cd^{3+}: blue).

(Fig. 4). For **3**, a broad blue-shifted emission from the Cd/L center can be detected at $\lambda_{max} = 440$ nm upon excitation of the ligand-centered absorption band at 380 nm. Complexes **1** and **2** show the visible emission bands of Eu^{3+} ($^5D_0 \rightarrow {}^7F_j$ transitions, $j = 0, 1, 2, 3$ and 4) and Tb^{3+} ($^5D_4 \rightarrow {}^7F_j$ transitions, $j = 6, 5, 4$ and 3) ions, respectively, while the Cd/L-centered emission is not detected (Fig. 4). The appearance of the symmetry-forbidden emission $^5D_0 \rightarrow {}^7F_0$ at 579 nm indicates that the Eu^{3+} ions in **1** occupy sites with low symmetry and have no inversion center.[17] This is in agreement with the result of the single-crystal X-ray analysis. It is also further confirmed by the intensity ratio of 3.8 for $I(^5D_0 \rightarrow {}^7F_2)/I(^5D_0 \rightarrow {}^7F_1)$, which is a good measure of the nature and symmetry of the first coordination sphere of Eu^{3+} ion.[18]

In **1** and **2**, there are no solvent molecules such as MeOH or H_2O coordinated to the lanthanide ions which could quench lanthanide luminescence. Also, the
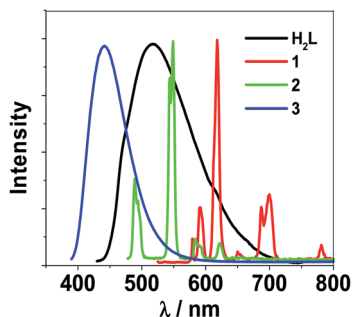
Fig. 4 Emission spectra of the free ligand H_2L and complexes **1–3** in CH_3CN at room temperature.

Ln(III) centers are shielded within the drum-like structures and therefore fairly well protected from the outside solvent environment. This shielding may help to improve their luminescent properties. The fluorescence quantum yields (Φ_{em}) of **1** and **2** are 0.277 and 0.093, respectively. These values are higher than those of polynuclear complexes and 1-D coordination polymers formed with the Schiff base ligands that feature shorter chain lengths between ends.[19] Interestingly, the Cd/L based emission is also observed as a broad band centered at about 540 nm for the larger 32-metal drums based on Er and Yb[10] while for the smaller drums based on Eu and Tb (**1** and **2**) the absence of Cd/L-centered luminescence in the emission spectra suggests that the L → Ln and Cd → Ln energy transfers take place efficiently.[20]
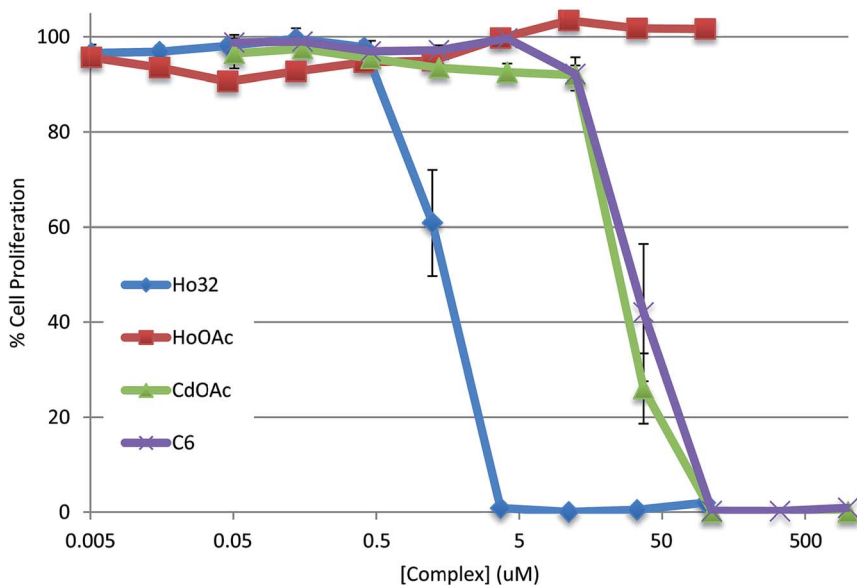

Fig. 5 Dose responsive cell proliferation curves of A549 lung cells treated with indicated complex. Error bars represent standard deviation.
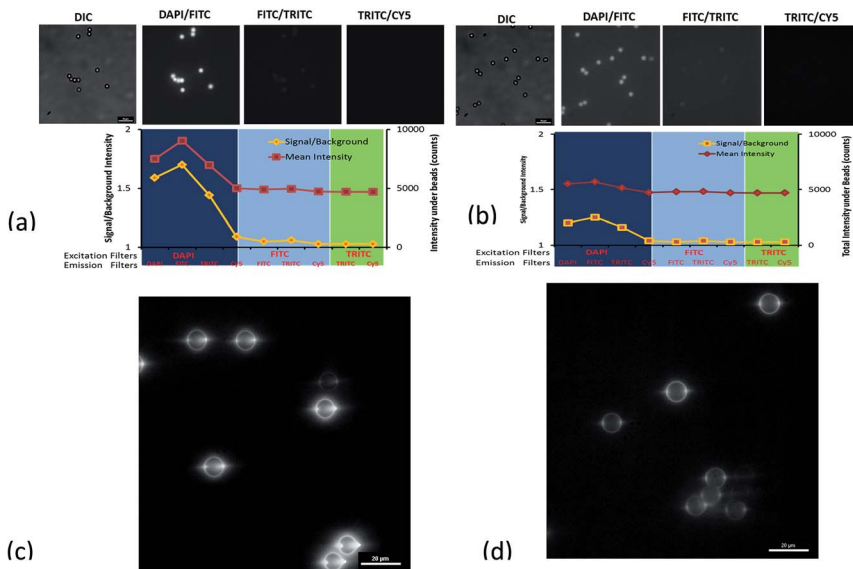
Fig. 6 Polystyrene beads doped with Er or Yb nano-drums show bright fluorescence under epifluorescent and total internal reflection fluorescence (TIRF) microscopy. Epifluorescence images of (a) Er or (b) Yb nano-drum-loaded polystyrene beads excited with an illumination source filtered by a DAPI filter. Images and associated signal/background intensities are displayed for the DAPI, FITC, TRITC and Cy5 emission filter channels. TIRF images of (c) Er or (d) Yb nano-drum-loaded polystyrene bead obtained by exciting at 405 nm.

3.3. Cytotoxicity screening

To determine the inherent cytotoxicity of the complexes, cell proliferation assays were conducted using A549 lung cancer cells and AGS gastric cancer cells using the holmium nano-drum, $[Ho_8Cd_{24}L_{12}(OAc)_{48}]$ (4), shown in Fig. 3. As shown in Fig. 5 for the A549 cells, 4 displayed an IC_{50} value of 1.32 ± 0.11 μM. A similar IC_{50} value was obtained for AGS cells, approximately 5 μM. Metal salt $Cd(OAc)_2 \cdot 2H_2O$ and the C6 ligand provided IC_{50} values of 31.0 ± 7.0 and 29.7 ± 1.2 μM, respectively, while $Ho(OAc)_3 \cdot 4H_2O$ displayed no inhibition of cell proliferation under the concentrations tested.

3.4. Microscopy studies

Crosslinked polystyrene beads (6 mm) containing either $[Er_8Cd_{24}L_{12}(OAc)_{48}]$ (5) or $[Yb_8Cd_{24}L_{12}(OAc)_{48}]$ (6) were visualized using epifluoresence, TIRF, and two-photon microscopy by observing emission in the visible spectrum. Using the epifluorescence platform, both bead types can be excited with an illumination source filtered with a DAPI filter. The bead images show high signal to background intensity and high mean intensity under the DAPI, FITC, TRITC and Cy5 emission filter channels (Fig. 6). The use of longer wavelength excitation filters did not result in significant emission from either bead type. The same beads exhibit high fluorescent signal with a 405 nm excitation laser with the TIRF imaging platform (Fig. 6). The two-photon fluorescence images shown in Fig. 7
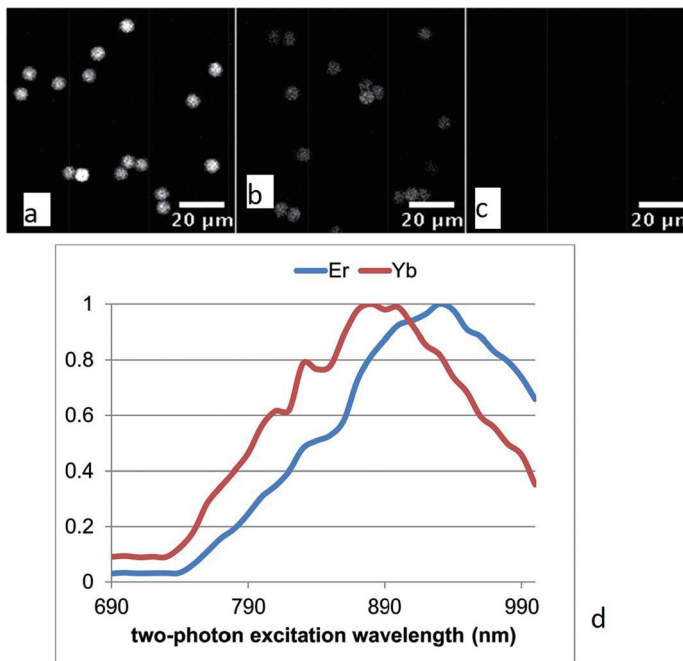
Fig. 7 Polystyrene beads loaded with Er and Yb nano-drums show bright fluorescence under two-photon fluorescence excitation microscopy. (a) Er- and (b) Yb-loaded poly-styrene beads were excited at 760 nm with constant laser power and detector sensitivity, with the images shown obtained by PMT with 535/50 nm emission filter. As a control, unloaded beads lack fluorescence (c). Normalized fluorescence intensity in the 535/50 nm emission channel is shown for when the laser is scanned from 690 to 1000 nm in 10 nm steps (d).

were acquired at constant laser power and detector sensitivity. Beads were excited at 760 nm, and the images shown were obtained by PMT with a 535/50 nm emission filter. Within this range, Er beads emitted with greater brightness than Yb beads upon two-photon excitation. Relative normalized fluorescence intensity in the 535/50 nm emission channel is shown for laser scans from 690 to 1000 nm in 10 nm steps. The Er (**5**) and Yb (**6**) nano-drum-containing beads display an excitation peak at 930 nm and 880 nm, respectively. In addition, beads loaded with either **5** or **6** were shown by XPS to contain Ln : Cd ratios of 1 : 3 (Fig. S7–S9 and Table S5†), consistent with the ratio revealed by single crystal X-ray studies.[10] Control beads lacking nano-drums did not display significant fluorescence in any of the microscopy studies presented here.

4. Discussion

The studies presented here explore the potential of a novel class of molecular lanthanide-based nanoparticles, called nano-drums, as bioprobes for biological imaging applications. Desirable features of a bioprobe include aqueous stability, thermodynamic stability and favourable photophysical properties, including narrow band emissions and no photobleaching.[5,21,22] Their crystal structures

reveal that these nano-drums are discrete multinuclear lanthanide clusters that self-assemble as homogeneous molecular species in a "drum" shape. The dimensions of these structures can be tuned at the molecular level, for example, by varying the anion, which changes the shape and composition of the nano-drum to yield a 24- or 32-metal cluster, but still yields a perfectly homogeneous particle size rather than a heterogeneous collection of different sized species. The changes that result from varying the anion also demonstrate the potential for enhancing emissions of this compound class in aqueous environments by caging or shielding the metal ions from solvents that could act as quenching agents. In addition, chemical modification of the flexible Schiff base linker with suitable functional groups may allow for further bioconjugation of the nano-drum.[23] Other modifications such as polyglutamation would also lead to enhanced aqueous solubility.[24]

Spectroscopic characterization of the nano-drums has also revealed that these molecules possess physical and chemical properties with potential for bioprobe development. ^{1}H NMR spectra remain unchanged for weeks, indicating that they are stable in solution, as well as in crystalline forms. In addition, polystyrene beads loaded with nano-drums could also be stored in aqueous buffer at room temperature for several months and still retain the imaging properties shown in Fig. 6 and 7. The photophysical properties of the nano-drums not only show the potential of these compounds as both visible and NIR-emitters,[10] but the presence of the Cd/L centre also allows their use as non-bleaching fluorescent labels that emit in the visible region of the spectrum and can be imaged using conventional, commercially available microscopy platforms. This added spectral flexibility cannot be attributed only to the photophysical properties of the Cd/L center; data indicate that the intensity of emission is significantly influenced by the presence of the lanthanide and that different lanthanides can enhance the emissive properties of these compounds. Of the two compounds imaged in beads, the Er nano-drum (**5**) displays a higher intensity visible emission spectrum compared to the Yb nano-drum (**6**) in solution (centered at 525 nm). This result is also consistent with the emissions from the beads observed by epifluorescence microscopy (Fig. 6). How the lanthanides modulate this emission is not well understood and demands further study.

To further explore the capacity of these nano-drums for applications in biological systems, we carried out cytotoxicity studies using two cancer cell lines. When corrected for the stoichiometries of the components within the assembled nano-drum (8 Ho, 24 Cd, 12 L), the IC_{50} of this compound lies in the range of 10–120 μM. This value is indicative of moderate to mild cytotoxicity and comparable to Eu(III) and Tb(III) molecular compounds that can be used as agents for cell imaging.[16,21] The mechanisms responsible for cellular uptake and cytotoxicity are not known at this point. Cellular uptake is likely to involve endocytosis and parameters influencing transport of these nano-drums into cells can include particle size, shape, surface chemistry, topology and mechanical properties.[25] Comparison of the cytotoxicity of compound **4** with components that form the assembled nano-drums suggest that the cytotoxic effects primarily originate from the Cd and ligand (L). These data are consistent with observations that the nature of the antenna (the Cd/L in the nano-drums) is the most important feature that controls toxicity in lanthanide bioprobes.[21]

Finally, the suitability of nano-drums for use in bioimaging applications was assessed using three microscopy platforms configured to detect fluorescence in the visible spectrum. As shown in Fig. 6 and 7, polystyrene beads loaded with these compounds could all be visualized by epifluorescence, TIRF or two-photon microscopy, and intensity scans of the beads showed spectral features consistent with previous data obtained on these compounds in solution.[10] In particular, the two-photon scan of the beads indicates a wide range for excitation, corresponding to a single photon excitation range maximum at 465 nm for the Er nano-drum (**5**) and 440 nm for the Yb nano-drum (**6**), This scan, along with other spectral data, explains why we can use the DAPI filter (340–380 nm) in the epifluorescence microscope and the 405 nm laser with the TIRF microscope to produce the fluorescence images presented here. These data also demonstrate that excitation in the visible region can be carried out with these compounds using conventional sources, in order to minimize damage to biological materials in situations where that is a genuine concern. However, excitation in the UV region (to induce NIR emission by the lanthanide) is also possible. Also, UV excitation is not a constraint when using the two-photon microscope, because excitation relies upon the absorption of two infrared photons simultaneously to permit imaging of living cells within intact tissues.

5.   Conclusions

The studies presented here show that this new class of self-assembling molecular nano-drums have considerable potential for use as imaging bioprobes for a range of platforms that use fluorescent or luminescent detection. Compared to conventional organic dyes or quantum dots used in biomedical applications, these bi-metal molecular compounds do not photobleach or blink. In addition, our nano-drums self-assemble as homogeneous nanoparticles with structurally accessible chemical moieties that are amenable to synthetic modification. The low temperature, bottom-up self-assembly route to these materials should allow for improvements in thermodynamic stability and photophysical properties of the nano-drums, as well as other important properties such as lanthanide shielding, solubility and toxicity. Chemical modifications to the Schiff base ligand are a precise way to tailor the properties of the nano-drum at the molecular level. Our future studies are focused on creating homogeneous molecular nanoparticles with bioconjugation capabilities. For example it should be possible to modify the flexible Schiff base ligand (H_2L) to bear functional groups such as thiol (–SH), isothiocyanate (–NCS), amino (–NH_2), and carboxylate (–CO_2H). Adding functional groups would lead to homogeneous molecular nano-drums with bioconjugation capabilities, while maintaining their advantageous photophysical properties. This work is in progress.

Acknowledgements

References

1 T. Kurkina and K. Balasubramanian, *Cell. Mol. Life Sci.*, 2012, **69**, 373.

2 C. L. Ventola, *P T*, 2012, **37**, 582.

3 M. R. Hartman, R. C. Ruiz, S. Hamada, C. Xu, K. G. Yancey, Y. Yu, W. Han and D. Luo, *Nanoscale*, 2013, **5**, 10141.

4 P. Tallury, A. Malhotra, L. M. Byrne and S. Santra, *Adv. Drug Delivery Rev.*, 2012, **62**, 424.

5 S. V. Eliseeva and J.-C. G. Bünzli, *Chem. Soc. Rev.*, 2010, **39**, 189.

6 S. U. Pandya, J. Yu and D. Parker, *Dalton Trans.*, 2006, 2757.

7 C. P. Montgomery, B. S. Murray, E. J. New, R. Pal and D. Parker, *Acc. Chem. Res.*, 2009, **42**, 925.

8 A. K. Hagan and T. Zuchner, *Anal. Bioanal. Chem.*, 2011, **400**, 2847.

9 X.-P. Yang, R. A. Jones and S. Huang, *Coord. Chem. Rev.*, 2014, **273–274**, 63–75.

10 X.-P. Yang, D. Schipper, R. A. Jones, B. J. Holliday and S. Huang, *J. Am. Chem. Soc.*, 2013, **135**, 8468.

11 F. Lam, J.-X. Xu and K.-S. Chan, *J. Org. Chem.*, 1996, **61**, 8414.

12 DENZO-SMN, Z. Otwinowski and W. Minor, in *Methods in Enzymology, 276: Macromolecular Crystallography*, ed. C. W. J. Carter, M. I. Simon and R. M. Sweet, Academic Press, 1997, p. 307, Part A.

13 G. H. Sheldrick, *SHELX 97, a software package for the solution and refinement of X-ray data*, University of Göttingen, Göttingen, Germany, 1997.

14 D. T. Cromer and J. T. Waber, *International Tables for X-Ray Crystallography*, Kynoch Press, Birmingham, 1974, vol. 4, table 2.2A.

15 (*a*) S. R. Meech and D. J. Philips, *J. Photochem.*, 1983, **23**, 193; (*b*) K. Nakamaru, *Bull. Chem. Soc. Jpn.*, 1982, **5**, 2697.

16 D. T. Thielemann, A. T. Wagner, E. Rösch, D. K. Kölmel, J. G. Heck, B. Rudat, M. Neumaier, C. Feldmann, U. Schepers, S. Bräse and P. W. Roesky, *J. Am. Chem. Soc.*, 2013, **135**, 7454.

17 (*a*) D. H. Metcalf, R. G. Ghirardelli and R. A. Palmer, *Inorg. Chem.*, 1985, **24**, 634; (*b*) M. Albin, R. R. Whittle and W. D. Horrocks, Jr, *Inorg. Chem.*, 1985, **24**, 4591.

18 (*a*) Q.-H. Xu, L.-S. Li, X.-S. Liu and R.-R. Xu, *Chem. Mater.*, 2002, **14**, 549; (*b*) Y. B. Katsimirski and N. K. Davidenko, *Coord. Chem. Rev.*, 1979, **27**, 223.

19 (*a*) X.-P. Yang, R. A. Jones and W.-K. Wong, *Chem. Commun.*, 2008, 3266; (*b*) X.-P. Yang, D. Lam, C. Chan, J. M. Stanley, R. A. Jones, B. J. Holliday and K.-W. Wong, *Dalton Trans.*, 2011, **40**, 9795.

20 (*a*) Y.-X. Chi, S.-Y. Niu, Z.-L. Wang and J. Jin, *Eur. J. Inorg. Chem.*, 2008, 2336; (*b*) J.-C. G. Bünzli and C. Piguet, *Chem. Soc. Rev.*, 2005, **34**, 1048; (*c*) S. Petoud, S. M. Cohen, J.-C. G. Bünzli and K. N. Raymond, *J. Am. Chem. Soc.*, 2003, **125**, 13324.

21 M. P. Coogan and V. Fernandez-Moreira, *Chem. Commun.*, 2014, **50**, 384.

22 J.-C. G. Bünzli, *Chem. Rev.*, 2010, **110**, 2729.

23 V. Biju, *Chem. Soc. Rev.*, 2014, **43**, 744.

24 T. V. Esipova, X. Yeb, J. E. Collins, S. Sakadzic, E. T. Mandeville, C. B. Murray and S. A. Vinogradov, *Proc. Natl. Acad. Sci. U. S. A.*, 2012, **109**, 20826.

25 I. Canton and G. Battaglia, *Chem. Soc. Rev.*, 2012, **41**, 2718.